Bull. Mater. Sci., Vol. 36, No. 2, April 2013, pp. 239–244. © Indian Academy of Sciences.

Hydrothermal synthesis of porous $Co(OH)_2$ nanoflake array film and its supercapacitor application

Z CHEN[a,*], Y CHEN[a], C ZUO[a], S ZHOU[a], A G XIAO[a] and A X PAN[b]

[a]College of Chemistry and Chemical Engineering, Hunan University of Arts and Science, Changde, Hunan 415000, China
[b]Department of Chemistry, Huzhou Teachers College, Huzhou 313000, China

MS received 31 January 2012; revised 17 April 2012

Abstract. **Porous α-$Co(OH)_2$ nanoflake array film is prepared by a facile hydrothermal synthesis method. The α-$Co(OH)_2$ nanoflake array film exhibits a highly porous net-like structure composed of interconnected nanoflakes with a thickness of 15 nm. The pseudo-capacitive behaviour of the $Co(OH)_2$ nanoflake array film is investigated by cyclic voltammograms (CV) and galvanostatic charge–discharge tests in 2 M KOH. The α-$Co(OH)_2$ nanoflake array film exhibits high capacitances of 1017 F g^{-1} at 2 A g^{-1} and 890 F g^{-1} at 40 A g^{-1} as well as rather good cycling stability for supercapacitor application. The porous architecture is responsible for the enhancement of the electrochemical properties because it provides fast ion and electron transfer, large reaction surface area and good strain accommodation.**

Keywords. **Cobalt hydroxide; hydrothermal synthesis; porous film; supercapacitor.**

1. Introduction

A new technology, the supercapacitor, has emerged with the potential to enable major advances in energy storage due to its fast recharge capability, long cycling life and high power performance (Miller and Simon 2008; Simon and Gogotsi 2008). Depending on the storage mechanism, supercapacitor is classified as an electrochemical double-layer capacitor (EDLC) or a pseudocapacitor (Zhang *et al* 2009). Early studies of supercapacitors mainly focus on EDLCs based on carbonaceous materials, which suffer from relatively low specific capacitance (<300 F g^{-1}) and instability at high charge–discharge rates (Liu *et al* 2010). In order to improve specific capacitance, lots of research has been dedicated for investigating pseudocapacitive materials such as hydroxides (Xia *et al* 2011a,b; Yuan *et al* 2011), oxides (Wu *et al* 2011a,b; Xia *et al* 2011a,b) and polymers (Wang *et al* 2011), which produce increased specific capacitances and high energy densities than carbonaceous materials. Among these available pseudocapacitive candidates, $Co(OH)_2$ is considered to be one of the most attractive materials owing to its high specific capacitance (theoretical specific capacitance up to 3560 F g^{-1}) (Cao *et al* 2004), well-defined electrochemical redox activity and low cost.

The pseudocapacitive performance of $Co(OH)_2$ is controlled by the kinetic features of the electrode. Porous nanostructured architectures are proved to be essential for obtaining high capacitance because porous nanostructures possess high specific surface area and short diffusion path lengths for ions and electrons, leading to fast kinetics, more efficient contact of electrolyte ions, and more electroactive sites for faradaic energy storage, resulting in high charge–discharge capacitances even at high current densities (Xia *et al* 2011a,b). Therefore, designing new electrodes with proper pore structure are highly desirable.

To date, a variety of methods have been developed to prepare nanostructured porous $Co(OH)_2$ films for high-performance supercapacitors, such as chemical precipitation (Xu *et al* 2011), electrochemical deposition (Gupta *et al* 2007; Kong *et al* 2011) and hydrothermal synthesis method (Jiang *et al* 2011). Despite this progress, most of these researches focus on $Co(OH)_2$ films grown by electrodeposition and leave more space for achieving the satisfactory cycle performance and high-rate capability of $Co(OH)_2$, particularly in terms of facile synthesis. Among these techniques, hydrothermal synthesis method is an advantageous technique due to its low cost, easy-processing and convenient for large-area growth. However, there are few reports devoted to pseudocapacitive characteristics of hydrothermal-synthesized porous $Co(OH)_2$ film except that prepared by Jiang *et al* (2011). Previously, Jiang *et al* (2011) reported α-$Co(OH)_2$ nanowire arrays on pyrolytic graphite via a hydrothermal synthesis method using NH_4F and $CO(NH_2)_2$ as the structure-directing agent and investigated their super-capacitor performance. In the present work, a facile hydrothermal synthesis method is put forward for the large-area growth of highly porous $Co(OH)_2$ nanoflake array film. The as-synthesized porous $Co(OH)_2$ nanoflake array film exhibits rather good pseudcapacitor properties with high capacitances and high-rate capabilities.

*Author for correspondence (xiaoanguo123@126.com)

2. Experimental

2.1 *Preparation of porous $Co(OH)_2$ nanoflake array film*

In a typical synthesis of the porous $Co(OH)_2$ nanoflake array film, 5 mmol of cobalt acetate ($Co(CH_3COO)_2$) and 15 mmol hexamethylenetetramine ($C_6H_{12}N_4$) were dissolved in 50 mL of distilled water to form homogeneous solution, which was transferred into teflon-lined stainless steel autoclave liners. After that, a piece of clean nickel foam substrate with $2 \times 5\,cm^2$ in size was immersed into the reaction solution. Then, the liner was sealed and maintained at 100 °C for 5 h in an electric oven. After the equipment cooled down to room temperature naturally, the sample was fetched out and rinsed with distilled water several times. The load weight of $Co(OH)_2$ film is approximately $1{\cdot}5\,mg\,cm^{-2}$.

2.2 *Characterization*

The morphology and structure of samples were characterized by X-ray diffraction (XRD, RIGAKU D/Max-2550 with CuKα radiation), field emission scanning electron microscopy (FESEM, FEI SIRION), high-resolution transmission electron microscopy (HRTEM, JEOL JEM-2010 F). The electrochemical measurements were carried out in a three-electrode electrochemical cell containing 2 M KOH aqueous solution as an electrolyte. Cyclic voltammetry (CV) measurements were performed on a CHI660c electrochemical workstation (Chenhua, Shanghai). CV measurements were carried out between −0·1 V and 0·6 V at 25 °C, $Co(OH)_2$ film grown on nickel foam as the working electrode, Hg/HgO as reference electrode and a Pt foil as counter-electrode. The film electrode with $0{\cdot}5 \times 1{\cdot}0\,cm^2$ in size was used for electrochemical impedance spectroscopy (EIS) measurements, which were made with a superimposed 5 mV sinusoidal voltage in the frequency range of 100 kHz–0·01 Hz. The galvanostatic charge–discharge tests were conducted on a LAND battery program-control test system. The as-prepared electrodes, together with a nickel mesh counter electrode and a Hg/HgO reference electrode were tested in a three-compartment system. The specific capacitance was calculated according to the following equation:

$$C = \frac{I\,\Delta t}{M\,\Delta V}, \tag{1}$$

where C ($F\,g^{-1}$) was specific capacitance, I (mA) represented discharge current and M (mg), ΔV (V) and Δt (s) designate mass of active materials, potential drop during discharge and total discharge time, respectively.

3. Results and discussion

The reactions involved in the hydrothermal synthesis of $Co(OH)_2$ can be illustrated as follows.

$$C_6H_{12}N_4 + 6H_2O \rightarrow 6HCHO + 4NH_3, \tag{2}$$

$$NH_3 + H_2O \leftrightarrow NH_4^+ + OH^-, \tag{3}$$

$$Co^{2+} + 2OH^- \rightarrow Co\,(OH)_2\,. \tag{4}$$

The as-deposited film is uniform in appearance and exhibits green in colour. XRD pattern of the as-prepared film is presented in figure 1. Except for the three representative peaks from nickel-foam substrate, other diffraction peaks are well indexed to layered α-$Co(OH)_2$ (JCPDS 74-1057). The hydrothermal-synthesized $Co(OH)_2$ film exhibits a highly porous structure with pore diameter ranging from 20–400 nm (figure 2(a and b)). The interconnected network is made up of freestanding nanoflakes with thickness of about 15 nm. This porous morphology is similar to those of electrodeposited $Co(OH)_2$ films reported by other authors (Gupta *et al* 2007; Chou *et al* 2008; Kong *et al* 2011). The preferential nanoflake growth is because of $Co(OH)_2$ crystal that has a layered brucite crystal structure of the CdI_2 type, which shows weak interaction between layers and strong binding within the layered planes. Neighbouring layers are bound together by weak Van der Waal forces. Therefore, its (0 0 1) plane is stable with the lowest surface energy (Xia *et al* 2010a,b). Thus, $Co(OH)_2$ will preferentially grow along the layered plane to form two-dimensional nanoflake film. To check the adherence of the $Co(OH)_2$ film to the nickel foam substrate, we have carried out a long-time ultrasonication test towards the $Co(OH)_2$ sample to examine the robust mechanical adhesion. The $Co(OH)_2$ nanoflake array film was immersed in distilled water and then received a sonication test for 30 min in the ultrasonication cleaner (power: 250 W; frequency: 40 KHz). Impressively, the $Co(OH)_2$ nanoflake array film does not detach from the nickel foam substrate and basically maintains the nanoflake array structure after sonication (figure 2(d)). It is indicated that the as-prepared $Co(OH)_2$ nanoflake array film has quite good mechanical

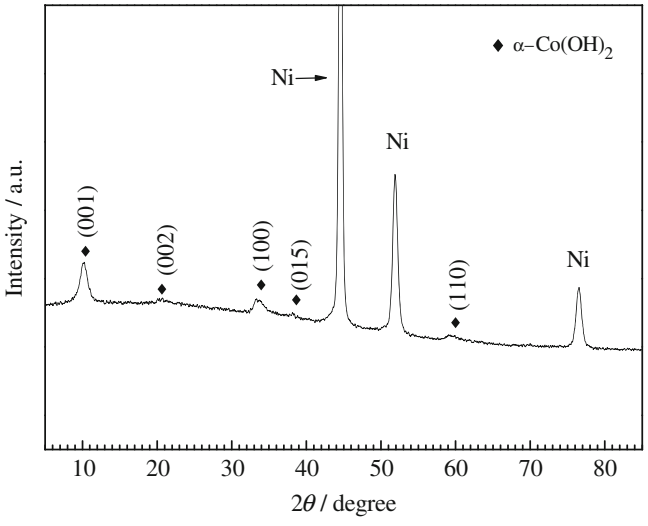

Figure 1. XRD pattern of film prepared by hydrothermal synthesis method.

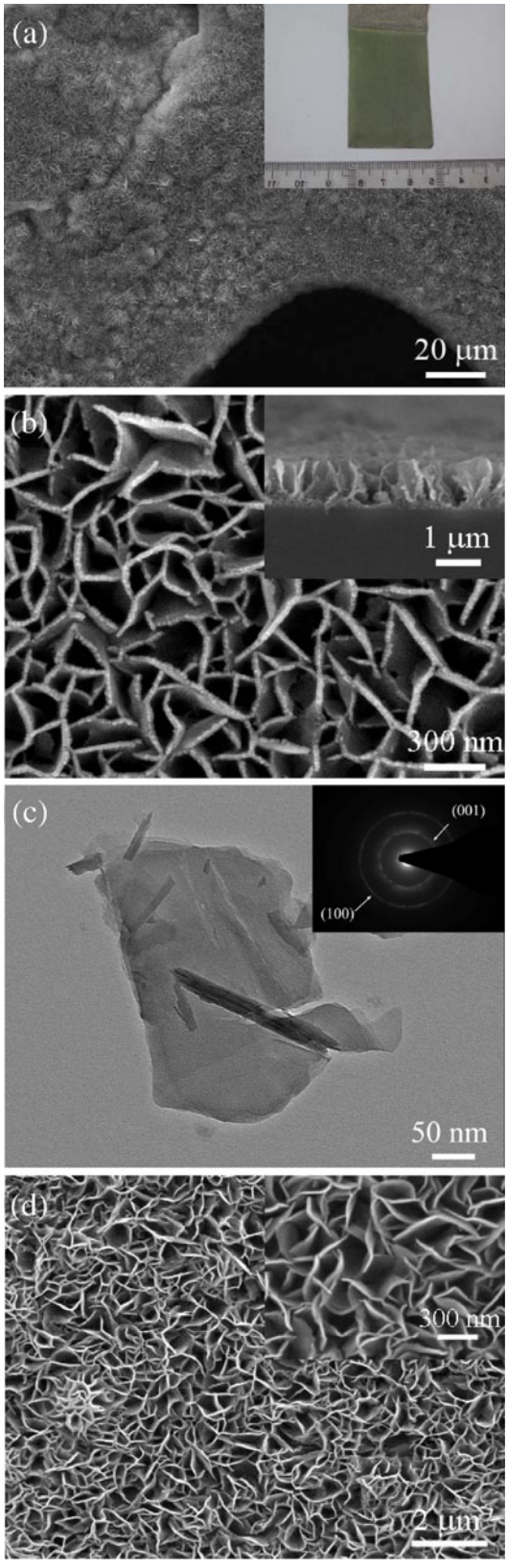

Figure 2. (**a**) and (**b**) SEM images of porous α-Co(OH)$_2$ nanoflake array film (photograph of sample in inset); (**c**) TEM image of α-Co(OH)$_2$ nanoflake (SAED pattern in inset) and (**d**) SEM image of Co(OH)$_2$ nanoflake array film after sonication for 30 min.

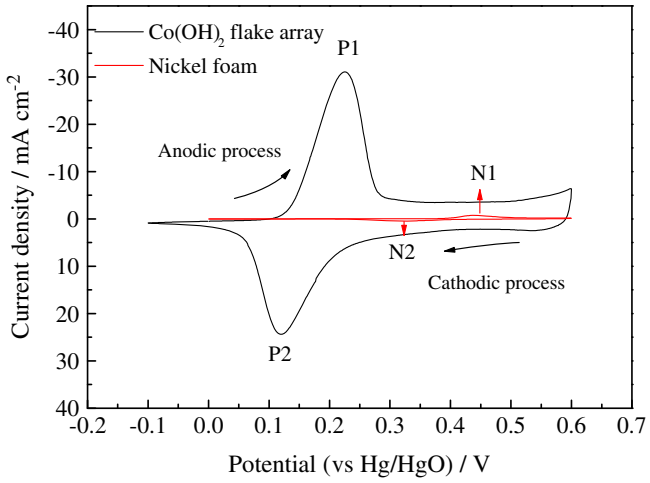

Figure 3. Cyclic voltammograms of porous α-Co(OH)$_2$ nanoflake array film and nickel foam in potential region of −0·1–0·6 V at a scanning rate of 10 mV s^{-1} at second cycle.

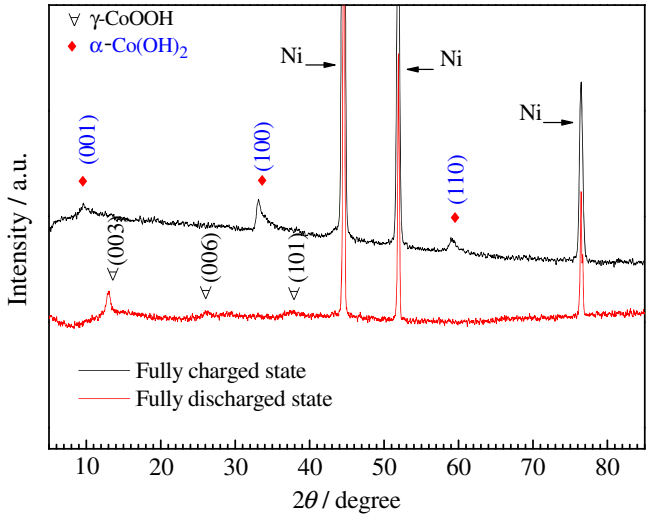

Figure 4. XRD patterns of porous α-Co(OH)$_2$ nanoflake array film at fully charged and discharged states at 10th cycle.

adhesion. It is believed that this porous feature is helpful to the enhancement of electrochemical properties because it would lead to fast ion/electron transfer, sufficient contact between active materials and electrolyte, and enhanced flexibility. TEM image shows that the individual nanoflake has a smooth texture (figure 2c). Additionally, all diffraction rings in the selected area electronic diffraction (SAED) pattern of the nanoflake can be indexed with the α-Co(OH)$_2$ phase, reflecting that the α-Co(OH)$_2$ nanoflake array film is polycrystalline in nature.

Figure 3 shows the CV curve of the Co(OH)$_2$ nanoflake array film at a scanning rate of 10 mV s^{-1}. A pair of strong redox couple $P1/P2$ is noticed in the CV curve, indicating

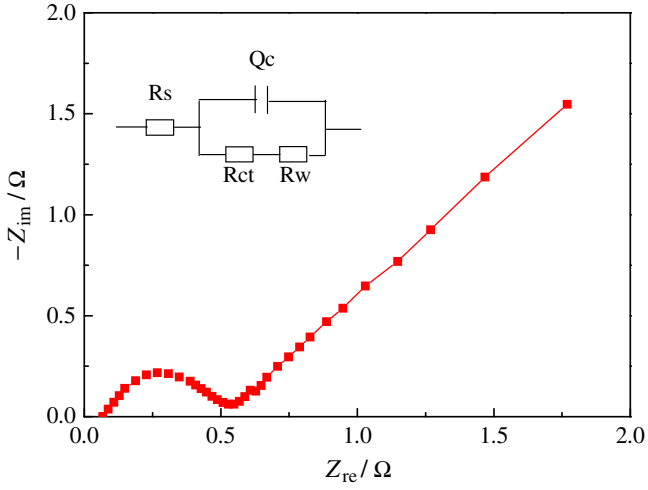

Figure 5. Nyquist plot of porous α-$Co(OH)_2$ nanoflake array film after 100% depth of discharge at 50th cycle.

that the capacitance characteristics is typical pseudocapacitance, distinct from that of the electric double-layer capacitance, which would produce a CV curve close to an ideal rectangular shape. The anodic peak is due to the oxidation of $Co(OH)_2$ to CoOOH and the cathodic peak is for the reverse process, expressed as follows (Zhou *et al* 2008; Chang *et al* 2009; Xia *et al* 2010a,b).

$$Co(OH)_2 + OH^- \leftrightarrow CoOOH + H_2O + e^-. \quad (5)$$

Generally, for $Co(OH)_2$ electrode material, two plausible redox processes could occur during the potential sweep. The redox couple at higher potential can be illustrated as follows (Zhou *et al* 2008; Chang *et al* 2009; Xia *et al* 2010a,b).

$$CoOOH + OH^- \leftrightarrow CoO_2 + H_2O + e^-. \quad (6)$$

It should be mentioned that only one redox couple $P1/P2$ is observed in our case, the second redox couple of conversion between CoOOH and CoO_2 does not appear. Similar phenomena have been reported by other authors (Gupta *et al* 2007; Zhou *et al* 2008). The difference in CV behaviour between our result and those in the literature is probably due to adopted different deposition conditions and different morphology structures. Meanwhile, the phases of films at the fully charge and discharge states are also investigated by XRD (figure 4). The film contains γ-CoOOH (JCPDS

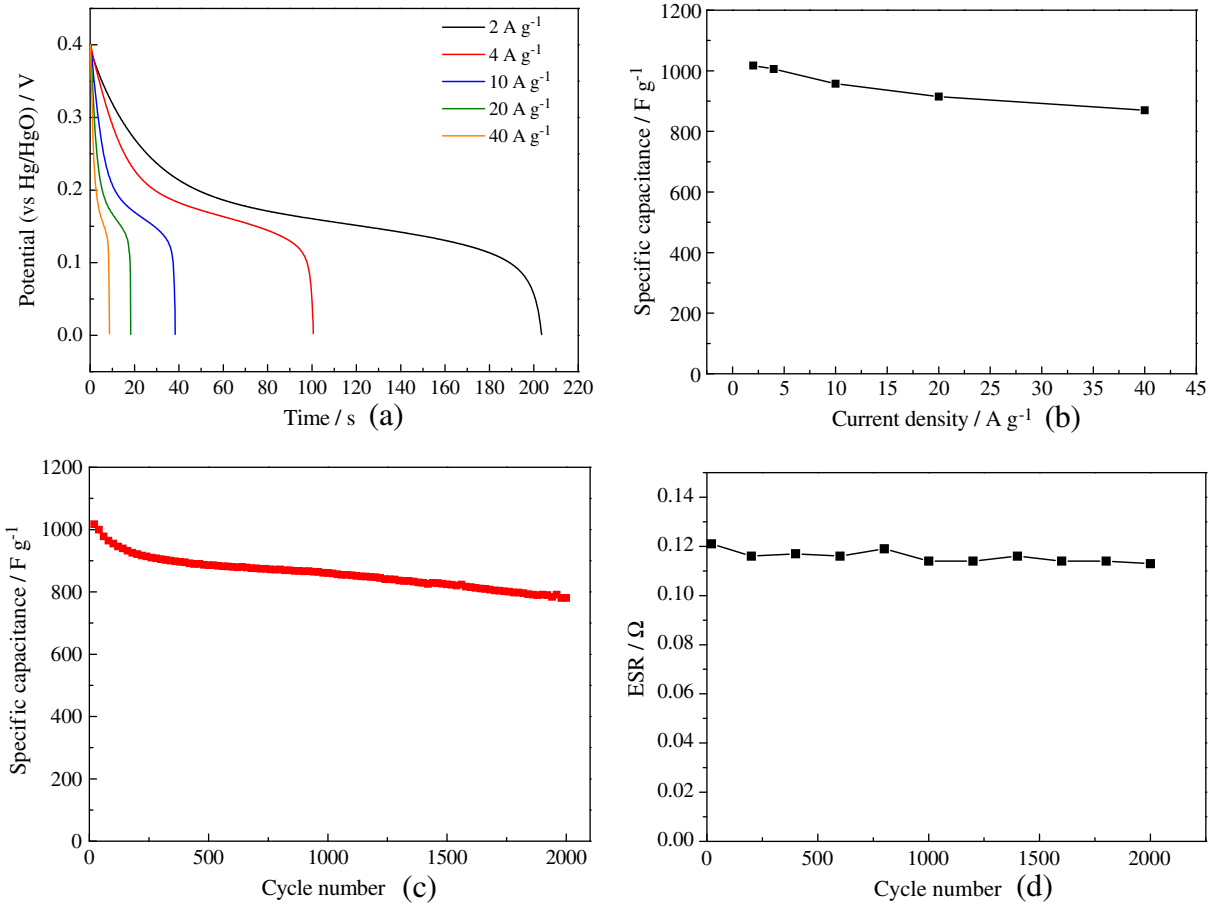

Figure 6. (**a**) Discharge curves of porous α-$Co(OH)_2$ nanoflake film at different discharge current densities and (**b**) corresponding capacitances; (**c**) cycling performance of porous α-$Co(OH)_2$ nanoflake array film at 2 A g^{-1} and (**d**) ESR variation of ESR of porous α-$Co(OH)_2$ nanoflake film with cycle number.

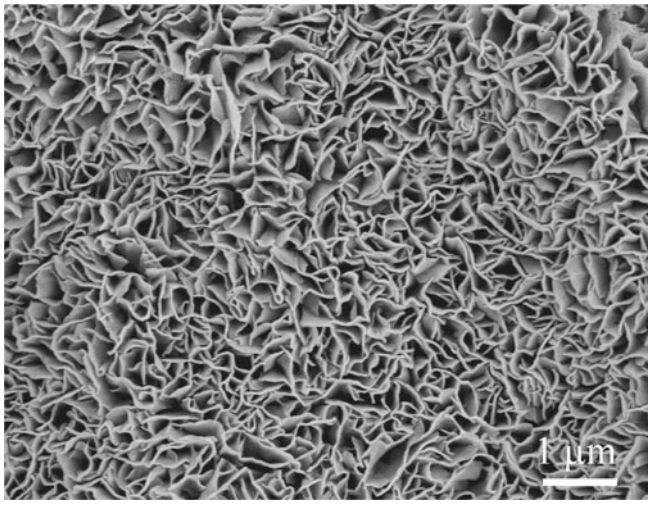

Figure 7. SEM image of fully discharged porous α-Co(OH)$_2$ nanoflake array film after 2000 cycles.

07-0169) phase at the fully charged state and α-Co(OH)$_2$ (JCPDS 74-1057) phase at the fully discharged state (Chang *et al* 2009). These XRD results are quite in agreement with the CV results. Besides, the nickel foam substrate also shows a redox process $N1/N2$, which is due to the reversible reaction of Ni(II)/Ni(III) formed on the nickel surface, but its peak current intensities are much lower than those of the Co(OH)$_2$ flake array film. Though the redox process $N1/N2$ will contribute to the specific capacitance of the film, its contribution is quite less than 3%.

The Nyquist plot of the Co(OH)$_2$ flake array is presented in figure 5. The EIS curve consists of a depressed arc in high-frequency regions and an inclined line in low-frequency regions. Generally, the semicircle reflects the electrochemical reaction impedance (R_ct) of the film electrode and the line indicates the diffusion of the electroactive species (R_w). R_S and Q_C designate the total ohmic resistance of solution and electrodes and the capacitance of the double layer. Generally, bigger semicircle means larger charge transfer resistance, and line with higher slope indicates lower ion diffusion rate. These parameters are calculated through the plots with ZView software. In our case, the values for R_ct, R_w, R_s and Q_c were measured to be 0·101, 0·193, 0·071 and 0·46 F, respectively.

The supercapacitor properties are also tested by galvanostatic charge–discharge measurements. Discharge curves of the porous α-Co(OH)$_2$ nanoflake array film and corresponding specific capacitances at various discharge current densities are shown in figure 6(a and b). The porous α-Co(OH)$_2$ nanoflake array film exhibits a pseudocapacitance of 1017 F g^{-1} at 2 A g^{-1}, 1006 F g^{-1} at 4 A g^{-1}, 957 F g^{-1} at 10 A g^{-1}, 915 F g^{-1} at 20 A g^{-1} and 890 F g^{-1} at 40 A g^{-1}, respectively. These values are higher than those obtained from porous Co(OH)$_2$ powder materials (<650 F g^{-1}) (Kong *et al* 2009; Yuan *et al* 2010), and comparable to those of porous electrodeposited Co(OH)$_2$ films (1084 F g^{-1}) (Zhou *et al* 2008), but lower than those from mesoporous Co(OH)$_2$ nanoflake (2646 F g^{-1}) films (Wu *et al* 2011a, b), and Co(OH)$_2$ nanoflakes grown on ultra-stable *Y* zeolite (3108 F g^{-1}) (Cao *et al* 2004).

The pretty good pseudocapacitive performance of the porous α-Co(OH)$_2$ nanoflake array is mainly due to the porous architecture. The nanoflakes with open spaces allow easy diffusion of ions among them and shorten diffusion paths for both electrons and ions within the oxides. Besides, the porous structure provides larger surface area and more active sites for electrochemical reactions. These features are particularly helpful for high-rate applications, resulting in rather good pseudocapacitive performance. The α-Co(OH)$_2$ nanoflake array film shows quite a good pseudocapacitance retention with 781 F g^{-1} after 2000 cycles maintaining 76·7% of the maximum value (figure 6(c)). In our case, the film was tested in three-electrode system, the equivalent series resistance keeps at about 0·1–0·125 Ω during the cycle (figure 6(d)). Figure 7 shows the SEM image of film after 2000 cycles. The α-Co(OH)$_2$ nanoflake array film keeps the structure integrity and the porous morphology is basically preserved, indicating that the porous structure could have good strain accommodation caused by volume expansion and keep structure stable.

4. Conclusions

In summary, a porous α-Co(OH)$_2$ nanoflake array film is prepared by a facile hydrothermal synthesis method. The α-Co(OH)$_2$ nanoflake array film exhibits a porous net-like structure composed of interconnected free-standing nanoflakes with thickness of about 15 nm. The α-Co(OH)$_2$ nanoflake array film has demonstrated good pseudocapacitive performance with high specific capacitance of 1017 F g^{-1} at 2 A g^{-1} and good cycling stability. The enhanced capacitive performance is mainly due to the high porosity and large surface area of the porous architecture. Additionally, the porous structure can relax the volume change caused by the electrochemical reaction and keep structure stable.

Acknowledgement

This work was supported by the construct program of the key discipline in Hunan province (Applied Chemistry).

References

Cao L, Xu F, Liang Y Y and Li H L 2004 *Adv. Mater.* **16** 1853

Chang Z R, Li H J, Tang H W, Yuan X Z and Wang H J 2009 *Int. J. Hydrogen. Energy* **34** 2435

Chou S L, Wang J Z, Liu H K and Dou S X 2008 *J. Electrochem. Soc.* **155** A926

Gupta V, Kusahara T, Toyama H, Gupta S and Miura N 2007 *Electrochem. Commun.* **9** 2315
Jiang J A, Liu J P, Ding R M, Zhu J H, Li Y Y, Hu A Z, Li X and Huang X T 2011 *Acs Appl. Mater. Interfaces* **3** 99
Kong L B, Liu M C, Lang J W, Liu M, Luo Y C and Kang L 2011 *J. Solid State Electr. Chem.* **15** 571
Kong L B, Lang J W, Liu M, Luo Y C and Kang L 2009 *J. Power Sources* **194** 1194
Liu C, Li F, Ma L P and Cheng H M 2010 *Adv. Mater.* **22** E28
Miller J R and Simon P 2008 *Science* **321** 651
Simon P and Gogotsi Y 2008 *Nat. Mater.* **7** 845
Wang G, Zhang L and Zhang J 2011 *Chem. Soc. Rev.* DOI: 10.1039/c1cs15060j
Wu C M, Fan C Y, Sun I W, Tsai W T and Chang J K 2011a *J. Power Sources* **196** 7828
Wu J B, Lin Y, Xia X H, Xu J Y and Shi Q Y 2011b *Electrochim. Acta* **56** 7163
Xia X H, Tu J P, Wang X L, Gu C D and Zhao X B 2010a *J. Power Sources* **195** 2014
Xia X H, Tu J P, Zhang J, Xiang J Y, Wang X L and Zhao X B 2010b *Acs Appl. Mater. Interfaces* **2** 186
Xia X H, Tu J P, Mai Y J, Wang X L, Gu C D and Zhao X B 2011a *J. Mater. Chem.* **21** 9319
Xia X H, Tu J P, Wang X L, Gu C D and Zhao X B 2011b *J. Mater. Chem.* **21** 671
Xu C H, Sun J and Gao L A 2011 *Crystengcomm* **13** 1586
Yuan C Z, Hou L R, Shen L F, Li D K, Zhang F, Fan C G, Li J M and Zhang X G 2010 *Electrochim. Acta* **56** 115
Yuan Y F, Xia X H, Wu J B, Yang J L, Chen Y B and Guo S Y 2011 *Electrochim. Acta* **56** 2627
Zhang Y *et al* 2009 *Int. J. Hydrogen Energy* **34** 4889
Zhou W J, Zhang J, Xue T, Zhao D D and Li H L 2008 *J. Mater. Chem.* **18** 905